BIOCHEMISTRY
including biophysical chemistry & molecular biology

Article

pubs.acs.org/biochemistry

New Paradigm for Allosteric Regulation of *Escherichia coli* Aspartate Transcarbamoylase

Gregory M. Cockrell, Yunan Zheng, Wenyue Guo, Alexis W. Peterson, Jennifer K. Truong, and Evan R. Kantrowitz*

Department of Chemistry, Boston College, Merkert Chemistry Center, 2609 Beacon Street, Chestnut Hill, MA 02467 U.S.A.

Supporting Information

ABSTRACT: For nearly 60 years, the ATP activation and the CTP inhibition of *Escherichia coli* aspartate transcarbamoylase (ATCase) has been the textbook example of allosteric regulation. We present kinetic data and five X-ray structures determined in the absence and presence of a Mg^{2+} concentration within the physiological range. In the presence of 2 mM divalent cations (Mg^{2+}, Ca^{2+}, Zn^{2+}), CTP does not significantly inhibit the enzyme, while the allosteric activation by ATP is enhanced. The data suggest that the actual allosteric inhibitor of ATCase in vivo is the combination of CTP, UTP, and a divalent cation, and the actual allosteric activator is a divalent cation with ATP or ATP and GTP. The structural data reveals that two NTPs can bind to each allosteric site with a divalent cation acting as a bridge between the triphosphates. Thus, the regulation of ATCase is far more complex than previously believed and calls many previous studies into question. The X-ray structures reveal that the catalytic chains undergo essentially no alternations; however, several regions of the regulatory chains undergo significant structural changes. Most significant is that the N-terminal region of the regulatory chains exists in different conformations in the allosterically activated and inhibited forms of the enzyme. Here, a new model of allosteric regulation is proposed.

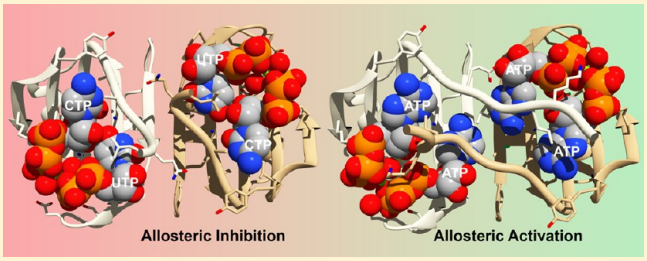

Numerous textbooks use *Escherichia coli* aspartate transcarbamoylase (ATCase; aspartate carbamoyl transferase; EC 2.1.3.2) to exemplify how an enzyme can control the rate of a metabolic pathway by altering its catalytic activity through allosteric regulation and homotropic cooperativity. In *E. coli*, ATCase catalyzes the committed step in pyrimidine nucleotide biosynthesis, the reaction between carbamoyl phosphate (CP) and L-aspartate (Asp) to form *N*-carbamoyl-L-aspartate and P_i.[1]

E. coli ATCase is composed of six chains (M_r 34 000) arranged into two trimers and six chains (M_r 17 000) arranged into three dimers. The two trimers contain the six active sites and are referred to as the catalytic subunits, while the three dimers contain the six allosteric sites and are referred to as the regulatory subunits. The holoenzyme can exist in two different structural forms, a low-activity, low-affinity T state and a high-activity, high-affinity R state. The T and R states of ATCase are in an equilibrium.[2] The substrate Asp in the presence of CP can shift the equilibrium to the R state in a concerted fashion.[3] Thus, the Asp saturation curve for ATCase exhibits homotropic cooperativity. Allosteric regulation of ATCase is commonly described as being feedback inhibited by the pyrimidine nucleotide CTP and activated by purine nucleotide ATP. However, ATCase is also known to be feedback inhibited by UTP, but only in the presence of CTP, and activated by Mg^{2+}·ATP.[4,5] Recent crystallography studies have suggested a more complex mode of regulation involving a dinucleotide allosteric site, which requires a divalent cation to function.[6,7] The allosteric inhibitors stabilize the T state, and the allosteric activator stabilizes the R state, but these allosteric effectors cannot induce the transition from the T to the R state, although they do alter the equilibrium between the two states.[8]

While numerous models for the allosteric regulation of ATCase have been proposed, none are consistent with all of the currently available data. London and Schmidt first proposed a model for the allosteric regulation of ATCase in 1972.[9] At that time, it was known that the allosteric effectors bound to the regulatory chains with a stoichiometry of approximately one nucleotide per regulatory chain,[10] and the allosteric inhibitor CTP and the allosteric activator ATP competed for the same binding site.[11] This model is inconsistent with the discovery that UTP could inhibit the enzyme but only in the presence of CTP.[4] The synergistic inhibition of ATCase by the combination of CTP and UTP reduces the enzyme activity by approximately 95%. Explanations for synergistic inhibition were proposed on the basis of enzyme X-ray structures, in a space group which contained two regulatory chains in the asymmetric unit. These structures showed structural asymmetry between the two regulatory chains that composed a regulatory dimer.[12] Furthermore, numerous binding studies showed that both CTP and ATP bind to the holoenzyme and the isolated

Received: August 30, 2013
Revised: October 9, 2013
Published: October 18, 2013

regulatory dimer with two different affinities. These experiments suggested that the binding of the nucleotides within one regulatory dimer was asymmetric.[10,13,14]

More detailed information about nucleotide binding to ATCase was obtained by the incorporation of an unnatural fluorescent amino acid close to the allosteric site of the enzyme.[15] Analysis of fluorescence binding isotherms indicated that CTP and UTP bind independently, suggesting that CTP and UTP do not compete for the same binding site.

The structure of the enzyme in the presence of UTP revealed that one UTP bound per regulatory chain; however, the site at which UTP bound was near but not overlapping the site at which ATP and CTP bound.[6] Cockrell and Kantrowitz[7] then used dCTP as a surrogate for CTP to determine the structure of the enzyme in the presence of both dCTP and UTP. This structure revealed that the allosteric site of each regulatory chain could bind two nucleotides simultaneously with a divalent cation between them (see Figure 1). CTP or dCTP bind in

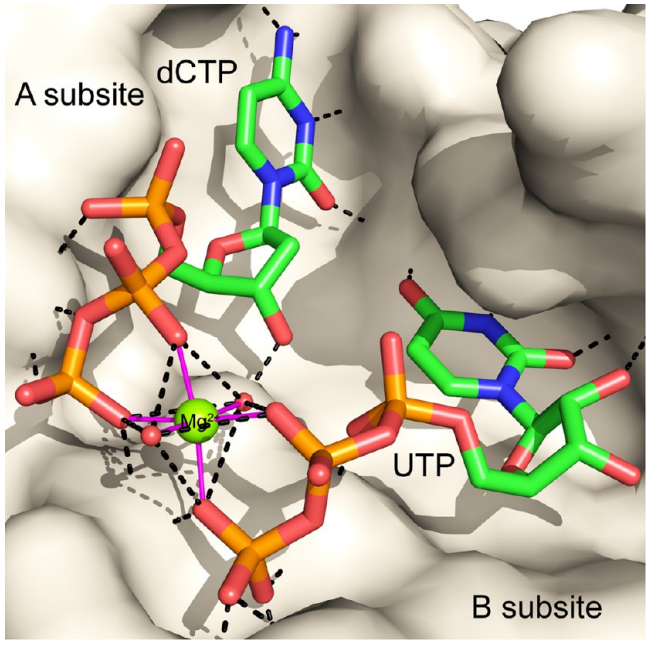

Figure 1. T-state X-ray crystal structure of ATCase in the presence of dCTP, UTP, and Mg^{2+}. The r6 regulatory subsites A and B are shown as a surface representation. dCTP is in the A subsite, and UTP is in the B subsite. The Mg^{2+} is shown as a green sphere, and coordinated ligand interactions are shown with magenta lines. Hydrogen-bonding interactions to the enzyme and waters are shown as dashed lines (black). Water ligands to Mg^{2+} are shown as red spheres. This figure was drawn with CHIMERA[49] using PDB ID 4FYX.[7]

essentially the same manner to the A subsite, and UTP binds to the B subsite. This work also showed that in the absence of divalent cations, UTP was unable to synergistically inhibit ATCase in the presence of CTP.

Two new factors must now be incorporated into any model for allosteric regulation of ATCase. First, each regulatory chain has not one but two sites capable of binding nucleotides, and second, a divalent cation such as Mg^{2+} influences enzyme activity by allowing the binding of nucleotides in the A and B subsites. Many of the past studies examining the kinetic and thermodynamic consequences of the addition of nucleotides to ATCase were performed under conditions in which the divalent cation concentration was unknown and/or not controlled. The omission of controlled divalent cation concentrations in previous experiments not only helps to explain the wide discrepancy in results,[10,13,14,16−18] but it also helps to explain the inability of previous investigations to detect the binding of nucleotides to the B subsite and correctly determine the stoichiometry of nucleotide binding. Here, we use kinetic studies to investigate the role of divalent cations on the allosteric regulation of ATCase. In addition, we use X-ray crystallography to determine five structures of the enzyme in the R state with nucleotides bound in the absence and presence of Mg^{2+}. These studies, in conjunction with previous work, allow us to propose a new model for the allosteric regulation of ATCase.

MATERIAL AND METHODS

Materials. Ampicillin, magnesium chloride hexahydrate, UTP, glycine, glucose, EDTA, agar, L-aspartate, *N*-carbamoyl-L-aspartate, 2-mercaptoethanol, and uracil were obtained from Sigma-Aldrich (St. Louis, MO). CTP and 2-bis(2-hydroxyethyl)amino-2-(hydroxymethyl)-1,3-propanediol (Bis-Tris) were from Santa Cruz Biotechnology, Inc. (Santa Cruz, CA). Tris, *N*-cyclohexyl-3-aminopropanesulfonic acid (CAPS), electrophoresis-grade acrylamide, enzyme-grade ammonium sulfate, and GTP were from MP Biomedicals (Santa Ana, CA). Antipyrine, diacetylmonoxime, sodium molybdate dihydrate, tryptone, and yeast extract were obtained from Fisher (Pittsburgh, PA). Casamino acid was from Becton, Dickinson and Company (Franklin Lakes, NJ). Agarose, ammonium persulfate, sodium dodecyl sulfate, coomassie brilliant blue, and Chelex 100 resin were purchased from Bio-Rad (Hercules, CA). The carbamoyl phosphate dilithium salt obtained from Sigma-Aldrich was purified before use by precipitation from 50% (v/v) ethanol and was stored desiccated at −20 °C.[19]

Enzyme Expression and Purification. *E. coli* ATCase was overexpressed in M9 media supplemented with 5 g/L casamino acids using *E. coli* strain EK1104[20] [F^- *ara*, *thi*, Δ(*pro-lac*), Δ*pyrB*, *pyrF*$^{\pm}$, *rpsL*] transformed with plasmid pEK152[21] containing the *E. coli pyrBI* gene. The isolation and purification was as previously described.[7] Enzyme concentrations were determined by absorbance measurements at 280 nm with an extinction coefficient of 0.59 cm^2/mg.[22]

Determination of ATCase Activity. Activity measurements with the nucleotide effectors ATP, CTP, GTP, and UTP were performed in the absence and presence of Mg^{2+}, Ca^{2+}, and Zn^{2+} at 28 °C. Pretreatment of nucleotides with Chelex 100 resin (Bio-Rad) was carried out to remove cation contamination in the commercial supply. Chelex 100 resin was added to each nucleotide solution (0.05 g per 1 mL). The mixture was stirred gently on ice for 1 h. Resin was removed by centrifugation, and the nucleotide solution with metal removed was obtained as supernatant. When required, $MgCl_2$, $CaCl_2$, or $ZnCl_2$ were added to adjust the M^{2+} concentration.

The concentration of the nucleotide triphosphates was determined spectrophotometrically at pH 7.0 using previously reported values of molar absorptivity.[23] The activity of the transcarbamoylase reaction was determined colorimetrically[24] in either 20 mM Bis-Tris, 20 mM Tris, and 20 mM CAPS pH 7.0 or 50 mM Tris pH 8.3, in the presence of a saturating concentration of carbamoyl phosphate (2.0 mM). Specific activity is in units of mM *N*-carbamoyl-L-aspartate·min^{-1}·mg^{-1}. Fitting of the experimental data to theoretical equations was accomplished by nonlinear regression.

dx.doi.org/10.1021/bi401205n | *Biochemistry* 2013, 52, 8036−8047

Crystallization, X-ray Data Collection, and Processing. *E. coli* ATCase (10 mg/mL) was placed in 50 μL dialysis buttons (Hampton Research, Aliso Viejo, CA) and dialyzed against 20 mL of crystallization buffer (50 mM maleic acid, 1 mM PALA, and 3 mM sodium azide, pH 5.90) at 20 °C.[25] Crystals formed in about 1 week with average dimensions of 0.6 × 0.2 × 0.2 mm. Dialysis buttons were transferred to 1 mL of crystallization buffer with either 5 mM CTP, 5 mM ATP, 5 mM each of ATP and $MgCl_2$, 5 mM each of UTP and $MgCl_2$, or 5 mM each of CTP, UTP, and $MgCl_2$, and allowed to equilibrate for 12 h. The crystals were dipped in crystallization buffer with 5 mM each of the matching nucleotide and $MgCl_2$ with 20% (v/v) 2-methyl-2,4-pentandiol as a cryoprotectant for approximately 1 min prior to flash freezing.

The data for the crystals soaked in CTP alone, UTP·Mg^{2+}, and ATP·Mg^{2+} were collected on beamline X29 at the National Synchrotron Light Source at Brookhaven National Laboratory (Upton, NY), while the data for crystals soaked in the presence of ATP alone and CTP·Mg^{2+}·UTP were collected with a Rigaku MicroMax-07 HF high-intensity microfocus rotating Cu anode X-ray generator coupled with Osmic VariMax Optics and a R-Axis IV^{++} image plate area detector that is part of the Boston College Crystallography Facility. The diffraction data were integrated, scaled, and averaged using either HKL2000[26] or d*TREK (Rigaku/MSC).[27]

Structure Solution and Data Refinement. Each structure was solved using phases from the R_{PALA} structure (PDB ID: 1D09)[28] as the initial model after removal of water and ligand molecules. Automated refinements using translation libration screw-motion (TLS) parameters were performed in PHENIX after an initial rigid body refinement.[29] Manual rebuilding, addition of waters, and nucleotide modeling were performed using COOT.[30] Waters were accepted if they were within hydrogen-bonding distance of main-chain or side-chain atoms. The final structures were validated using MolProbity[29] and PROCHECK.[31] Coordinates and structure factors for the R_{PALA}·ATP, R_{PALA}·CTP, R_{PALA}·UTP·Mg^{2+}·UTP, R_{PALA}·ATP·Mg^{2+}·ATP, and R_{PALA}·CTP·Mg^{2+}·UTP complexes have been deposited in the Protein Data Bank under accession codes 4KGV, 4KGX, 4KGZ, 4KH0, and 4KH1, respectively.

Calculation of Small-Angle X-ray Scattering Profiles. X-ray scattering patterns were calculated from the experimental X-ray crystal data using the fast SAXS profile computation with Debye formula (FOXS) server (http://modbase.compbio.ucsf.edu/foxs). The FoXS server explicitly computes all interatomic distances as well as models the first solvation layer on the basis of the atomic solvent accessible areas.[32] Hydrogen atoms were considered implicitly. For consistency, the first nine residues of each regulatory chain were not included in the calculations.

RESULTS AND DISCUSSION

Influence of Mg^{2+} on the Allosteric Response of ATCase. Although it has been known for almost 50 years that divalent cations influence the allosteric regulation of ATCase,[5,33,34] the mechanism by which divalent cations alter the allosteric response has remained elusive. In fact, under a physiological concentration of ATP, 3.6 mM,[35] Mg^{2+}·ATP activates ATCase 2.9-fold as compared to 1.9-fold for ATP alone.[5] Kung et al.[36] have estimated that the intracellular concentrations of Mg^{2+} and Ca^{2+} are greater than 20 mM and Zn^{2+} about 5-fold lower; however, the concentrations of these ions not complexed would be significantly lower. Since the dissociation constant of M^{2+}·NTP complexes is in the micromolar range, most of the NTPs in the cell will be present as M^{2+}·NTP complexes. Therefore, it is more reasonable to consider how ATCase responds to the NTPs in the presence rather than the absence of divalent cations.

To ensure that the NTPs did not contain trace amounts of divalent cations, all NTP solutions were pretreated. In order to directly compare our data to that of Wild et al.,[4] we used identical buffer, pH, and Asp concentrations. Figure 2 and Table 1 show the influence of Mg^{2+} on the activity of the enzyme in the presence of various NTPs and NTP combinations. Complete substrate saturation curves are shown in Figure 3.

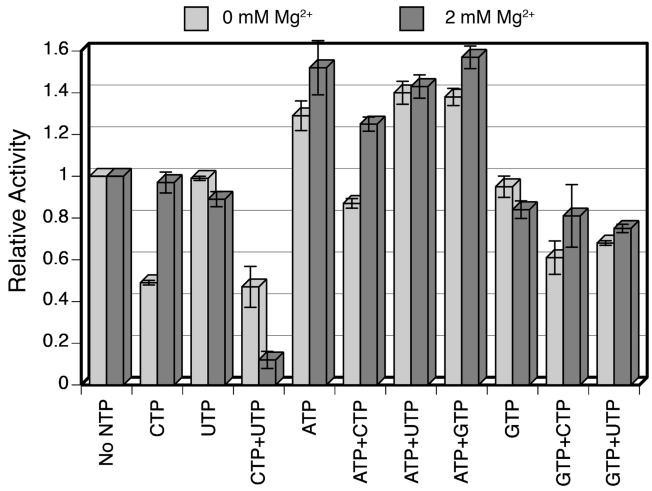

Figure 2. Influence of allosteric effectors on the activity of ATCase in the absence and presence of Mg^{2+} at pH 7. Relative activity was determined in the absence (light gray) or presence of 2 mM Mg^{2+} (dark gray). Measurements with single nucleotides were performed at 2 mM, while measurements with pairs were performed at 1 mM each. Assay conditions were identical to those used by Wild et al.[4] except that the NTPs were treated to remove trace metals before use. Data used for this figure are provided in Table 1

CTP can inhibit ATCase in the absence of Mg^{2+}; however, CTP has little influence on activity in the presence of 2 mM Mg^{2+}, suggesting a reduced role of CTP in the allosteric regulation of ATCase in vivo. However, in the presence of Mg^{2+}, the combination of the two end products of the pyrimidine pathway, CTP and UTP, inhibit the enzyme almost completely. It is known that CTP competitively inhibits its own production by binding to CTP synthetase, which would elevate the levels of UTP.[4] The combination of CTP, UTP, and Mg^{2+} as the natural allosteric inhibitor of ATCase would help to maintain an overall balance in relative pyrimidine and purine nucleotide pools without disrupting the balance between the CTP and UTP pools.

ATP is able to activate the enzyme in the absence of Mg^{2+}; however, in the presence of Mg^{2+}, ATP activates the enzyme to a greater extent (Figure 2). Furthermore, using small-angle X-ray scattering in solution, Fetler et al.[5] have reported that the R-state enzyme undergoes a significantly larger structural change with ATP in the presence of Mg^{2+} than in its absence. ATP and GTP activate the enzyme slightly more than ATP alone (see Figure 2). However, at higher concentrations of Asp, the addition of GTP to ATP and Mg^{2+}substantially increases the activity (see Figure 3). Buckstein et al.[35] have determined concentrations of ATP, GTP, UTP, and CTP in midlog phase

dx.doi.org/10.1021/bi401205n | *Biochemistry* 2013, 52, 8036−8047

Table 1. Influence of Allosteric Effectors on the Relative Activity[a] of ATCase in the Absence and Presence of Mg^{2+}

		Mg^{2+} (mM)[d]		
NTP[b]	reported value[c]	0	1.0	2.0
none	1.0	1.0	1.0	1.0
ATP	1.35	1.29 ± 0.07	1.33 ± 0.07	1.52 ± 0.13
CTP	0.43	0.49 ± 0.01	0.80 ± 0.05	0.97 ± 0.05
UTP	0.95	0.99 ± 0.01	0.97 ± 0.01	0.89 ± 0.04
GTP	0.71	0.95 ± 0.05	0.61 ± 0.06	0.84 ± 0.04
ATP + CTP	0.85	0.87 ± 0.02		1.25 ± 0.03
ATP + UTP	1.52	1.40 ± 0.06		1.43 ± 0.06
ATP + GTP	1.58	1.38 ± 0.04		1.57 ± 0.05
CTP + UTP	0.06	0.47 ± 0.10		0.12 ± 0.04
CTP + GTP	0.58	0.61 ± 0.08		0.81 ± 0.15
UTP + GTP	0.84	0.68 ± 0.01		0.75 ± 0.02

[a]Relative activity was determined by dividing the value of the specific activity of ATCase in the presence of nucleotide(s) by that in the absence of nucleotide(s). [b]All nucleotide concentrations were 2 mM. [c]The relative activities reported by Wild et al.[4] [d]All experiments were performed at 28 °C in 20 mM Bis-Tris, 20 mM Tris, and 20 mM CAPS buffer, pH 7.0 at saturating carbamoyl phosphate (2 mM) and 5 mM aspartate. The values reported are the average of four determinations.

E. coli to be 3.56, 1.66, 0.67, and 0.33 mM, respectively. These intracellular concentrations suggest that both end products of purine nucleotide biosynthesis, ATP and GTP, are involved in the allosteric regulation of ATCase.

These results are most relevant due to the high intercellular Mg^{2+} concentration; however, other divalent cations such as Ca^{2+} and Zn^{2+} were also found to cause very similar nucleotide responses as Mg^{2+} (see Table S1).

Structures of ATCase with NTPs in the Presence and Absence of Mg^{2+}. Five structures of ATCase were determined in the presence of *N*-phosphonacetyl-L-aspartate (PALA) to induce the R state. The ATP (R_{PALA}·ATP) and CTP (R_{PALA}·CTP) structures were determined in the absence of divalent cations as controls. The remaining three structures are NTP and Mg^{2+} combinations, including ATP·Mg^{2+}, CTP·UTP·Mg^{2+}, and UTP·Mg^{2+}, of which activates, inhibits the enzyme to the greatest extent, and has little influence on activity, respectively. A summary of the data collection and refinement statistics are provided in Table 2.

The addition of any NTP independent of the presence of Mg^{2+} induces almost no structural alterations to the catalytic chains. As shown in Table S2, the average RMSD between the catalytic chains of the R_{PALA} structure and the catalytic chains of each of the NTP structures determined was only 0.69 ± 0.05 Å. In contrast, the average RMSD between the regulatory chains of the R_{PALA} structure and the regulatory chains of each of the NTP structures determined was 1.41 ± 0.16 Å. Thus, the binding of the nucleotides has a significantly larger structural influence on the regulatory than the catalytic chains. The addition of any NTP with or without Mg^{2+} induces larger alterations in the r6 chains (RMSD 1.04 ± 0.28 Å) than the r1 chains (0.77 ± 0.07 Å), reinforcing the previously observed asymmetry in the regulatory dimer.[12]

During the T to R allosteric transition, the enzyme expands by approximately 11 Å along the 3-fold axis, as well as rotates around the 2- and 3-fold axes. The vertical separation[37] of ATCase is a measure of the distance between the centers of mass of the upper and lower catalytic trimers. The vertical

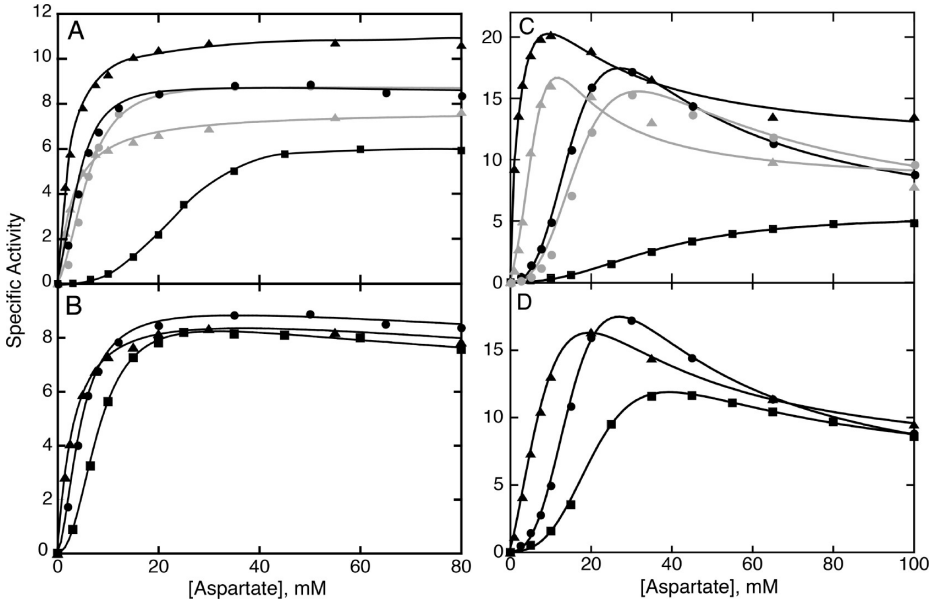

Figure 3. Asp saturation curves in the presence of NTPs and Mg^{2+} at pH 7.0 (A,B) and pH 8.3 (C,D). (A,C) Data are shown in the absence of NTPs and in the absence (circle, black) or presence of 2 mM Mg^{2+} (circle, gray), in the presence of 2 mM CTP, 2 mM UTP, and 2 mM Mg^{2+} (square, black), in the presence of 2 mM ATP, 2 mM GTP, and 2 mM Mg^{2+} (triangle, black), and in the presence of 4 mM ATP and 2 mM Mg^{2+} (triangle, gray). (B,D) Asp saturation curves in the absence (circle) and presence of ATP (triangle) and CTP (square) in the absence of Mg^{2+}. Specific activity, mM carbamoyl aspartate·min^{-1}·mg^{-1}, at 28 °C was determined colorimetrically at a saturating concentration of carbamoyl phosphate (2 mM) and 2 mM $MgCl_2$ in 20 mM Bis-Tris, 20 mM Tris, and 20 mM CAPS pH 7.0 or 50 mM Tris pH 8.3.

dx.doi.org/10.1021/bi401205n | *Biochemistry* 2013, 52, 8036−8047

Table 2. Data Collection and Refinement Statistics[a]

	R_{PALA}·ATP	R_{PALA}·CTP	R_{PALA}·UTP·Mg^{2+}·UTP	R_{PALA}·ATP·Mg^{2+}·ATP	R_{PALA}·CTP·Mg^{2+}·UTP
data collection statistics					
PDB entry	4KGV	4KGX	4KGZ	4KH0	4KH1
space group	*P*321	*P*321	*P*321	*P*321	*P*321
wavelength	1.542	1.075	1.075	1.075	1.542
cell dimensions					
a = *b*, *c* (Å)	121.1, 155.5	121.2, 154.7	121.4, 155.1	121.1, 155.1	120.9, 154.7
α, *β*, *γ* (°)	90, 90, 120	90, 90, 120	90, 90, 120	90, 90, 120	90, 90, 120
resolution (Å)	38.4−2.1 (2.2−2.1)	50−2.2 (2.3−2.2)	50−2.4 (2.5−2.4)	50−2.25 (2.33−2.25)	31.8−2.2 (2.3−2.2)
R_{sym}[b]	0.05 (0.38)	0.08 (0.65)	0.11 (0.68)	0.09 (0.74)	0.04 (0.37)
average (I/*σ*)	12.8 (3.3)	19.9 (3.9)	14.6 (3.7)	21.8 (3.7)	17.8 (3.8)
completeness (%)	100.0 (100.0)	100.0 (99.9)	100.0 (100.0)	100.0 (100.0)	99.4 (100.0)
redundancy	5.3 (5.3)	22.4 (18.9)	24.1 (21.2)	24.1 (22.0)	5.7 (5.6)
refinement statistics					
resolution (Å)	38.4−2.1	49.7−2.2	49.8−2.4	49.7−2.25	31.8−2.2
reflections	77 282	67 081	52 387	62 983	66 367
R_{work}/R_{free}	0.168/0.208	0.156/0.192	0.165/0.203	0.168/0.208	0.163/0.196
number of atoms					
protein	7098	7082	7074	7202	7132
waters	688	683	339	467	458
RMS deviations					
bond lengths (Å)	0.007	0.007	0.009	0.007	0.008
angles (°)	1.07	1.07	1.09	1.13	1.08
mean B value (Å^2)	48.3	39.3	56.9	48.2	60.2

[a]Values in parentheses are for the highest resolution shell. [b]$R_{sym} = \sum|(I - \langle I \rangle)|/\sum(I)$, where *I* is the observed intensity.

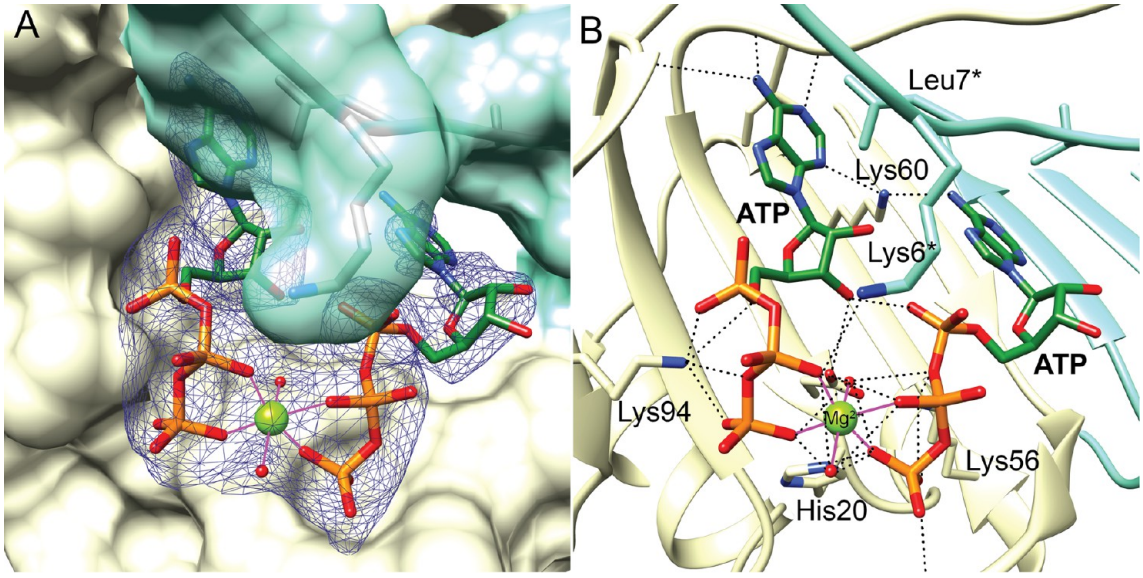

Figure 4. Allosteric site of ATCase with ATP and Mg^{2+}. (A) Surface representation of the r6 regulatory site with the r1 chain in blue (with transparency) and the r6 chain in yellow. Shown in dark blue is the electron density map at 2.5 *σ* calculated by omitting the atoms of the two ATPs, Mg^{2+}, and waters. (B) Same view as in (A) showing the interactions between the two ATPs and Mg^{2+} with the enzyme. Residues with asterisks are from the r1 chain.

separation of the T-state structure (PDB code 1ZA1) is 47.3 Å compared to 57.9 Å for the R-state structure (R_{PALA}, PDB code 1D09). The corresponding vertical separations for the R_{PALA}·ATP, R_{PALA}·CTP, R_{PALA}·UTP·Mg^{2+}·UTP, R_{PALA}·ATP·Mg^{2+}·ATP, and R_{PALA}·CTP·Mg^{2+}·UTP are 57.5, 57.2, 57.4, 57.4, and 57.3 Å, respectively. Thus, the quaternary structure of all the structures determined here have the characteristic vertical separation of the R state of ATCase. None of the NTPs in the absence or presence of Mg^{2+} cause an appreciable alteration in the quaternary structure of the enzyme.

The binding of the various NTP·Mg^{2+} combinations did not induce any significant alterations to the positions of side chains in the active site, although this may be due to the high affinity of PALA orienting the active site residues. Since the NTP·Mg^{2+} combinations do not significantly alter the activity of the enzyme at saturating concentrations of the substrates (see Figure 3), either the presence of PALA in the active site masks any conformational changes or the NTPs alter the enzyme activity by binding to the allosteric site and preferentially stabilizing the T or R states.

dx.doi.org/10.1021/bi401205n | *Biochemistry* 2013, 52, 8036−8047

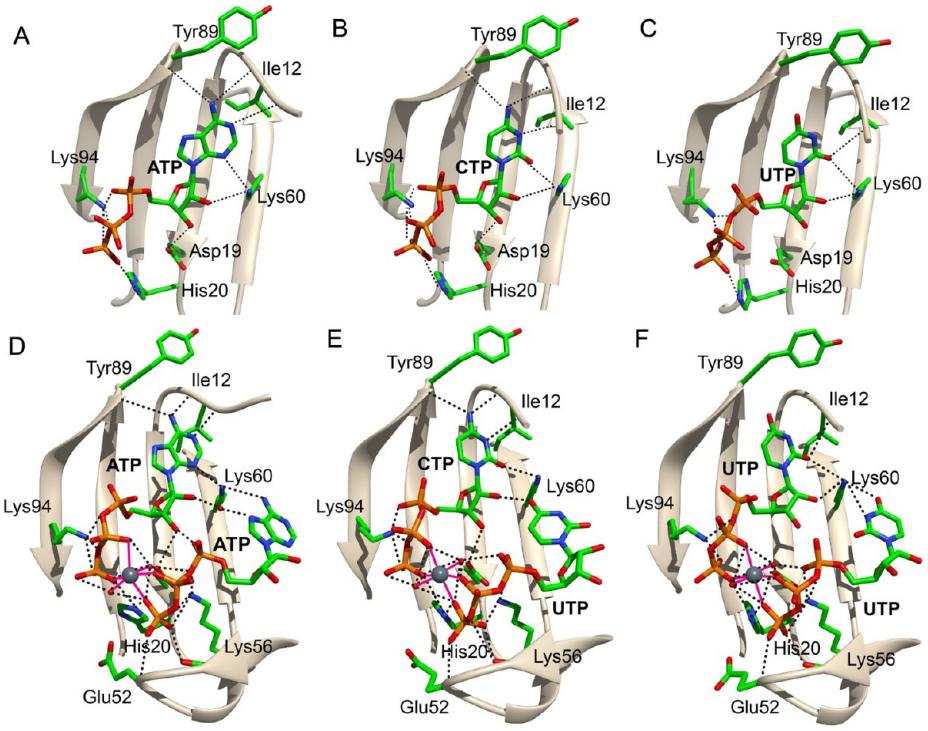

Figure 5. (Top) Structural comparison of ATP, CTP, and UTP bound in the A subsite. ATP (A), CTP (B), and UTP (C) are shown in the A subsite of the r6 regulatory domain of ATCase. In the case of UTP (C), the A subsite is only occupied in the presence of Mg^{2+} (not shown). Hydrogen-bonding interactions are shown as dash lines (black). (Bottom) Structural comparison of the allosteric site with Mg^{2+} and NTPs. The r6 regulatory chain of ATCase with (D) ATP·Mg^{2+}ATP, (E) CTP·Mg^{2+}·UTP, and (F) UTP·Mg^{2+}·UTP bound in the A and B subsites. For clarity, Asp19 is shown but not labeled. The Mg^{2+} is shown as a gray sphere, and coordinated ligand interactions are shown with magenta lines. Hydrogen-bonding interactions are shown as dashed lines (black). Water ligands to Mg^{2+} are shown as red spheres. For clarity, the first 10 residues of each regulatory chain are not shown. This figure was generated using CHIMERA.[49]

All the structures reported in the presence of Mg^{2+}, R_{PALA}·ATP·Mg^{2+}·ATP, R_{PALA}·CTP·Mg^{2+}·UTP, and R_{PALA}·UTP·Mg^{2+}·UTP show electron density in the allosteric site, corresponding to nucleotides bound in both the A and B subsites with a Mg^{2+} between. As an example, shown in Figure 4 is the r6 allosteric site of the R_{PALA}·ATP·Mg^{2+}·ATP structure, and additional detail can also be seen in Figure S1. The Mg^{2+} is octahedrally coordinated to six oxygen atoms, two from water molecules and one from the β-phosphate and the γ-phosphate of each of the two NTPs in the A and B subsites. The water molecules coordinated to the Mg^{2+} have additional stabilizing interactions with β and γ phosphate oxygens (see Figure 4B). Thus, the allosteric site of ATCase has two subsites capable of binding NTPs. As seen in Figure 5A,B, only one subsite is filled in the absence of a divalent cation. ATP and CTP bind competitively to the A subsite, while UTP binds only to the B subsite, as previously reported.[6] Previous studies have shown that the concentration of CTP necessary to half inhibit the enzyme is approximately 6-fold lower than the concentration of ATP needed to activate the enzyme.[38] The higher affinity of the enzyme for CTP compensates for the approximately 10-fold higher concentration of ATP in cells,[35] allowing the two nucleotides to compete more effectively.

Examination of the R·ATP·Mg^{2+}·ATP reveals that the interactions between the enzyme and ATP in the A subsite are very similar to those between the enzyme and ATP in the R_{PALA}·ATP structure determined in the absence of Mg^{2+} (compare Figure 5A,D). The phosphates of ATP bound in the B subsite interact with the backbone nitrogen of Glu52 as well as the side chains His20, Ser50, and Lys56, all of which are involved in the binding of UTP in the B subsite (compare Figure 5D,F). The ε-amino of Lys60 exhibits a water-mediated interaction and a polar interaction with N7 and the 6-amino group of the adenine ring, respectively (Figure 5D). However, in the B subsite of the adjacent regulatory chain there is a direct interaction between Lys60 and N7.

The allosteric site of the R_{PALA}·CTP·Mg^{2+}·UTP structure is shown in Figure 5E. CTP was modeled into the A subsite, and UTP was modeled into the B subsite on the basis of the subsite specificity previously determined.[7] The 4-amino group of the cytosine in the A subsite acts as a hydrogen bond donor to the backbone carbonyls of Ile12 and Tyr89. Furthermore, all the interactions to CTP observed in the R_{PALA}·CTP structure in the absence of Mg^{2+} are also observed in the R_{PALA}·CTP·Mg^{2+}·UTP structure (compare Figure 5B,E).

The allosteric site of the R_{PALA}·UTP·Mg^{2+}·UTP structure is shown in Figure 5F with UTP bound in both the A and B subsites. The interactions of UTP in the A subsite are different from those observed for CTP in the A subsite (compare Figure 5E,F). In the R_{PALA}·UTP·Mg^{2+}·UTP structure, the triphosphate portion of UTP in the A subsite makes the same interactions with His20 and Lys94, as do ATP and CTP. However, comparing the interactions between the pyrimidine rings of CTP and UTP, UTP has only half the number of interactions that CTP has in the A subsite. There is a polar interaction between Lys60 and the 2-keto oxygen of both CTP and UTP, but the 4-keto group of UTP is unable to hydrogen bond with the backbone carbonyls of Tyr89 and Ile12. Since the pyrimidine ring of UTP is not held as strongly, it is somewhat displaced relative to CTP, which may explain the inability of

dx.doi.org/10.1021/bi401205n | *Biochemistry* 2013, 52, 8036−8047

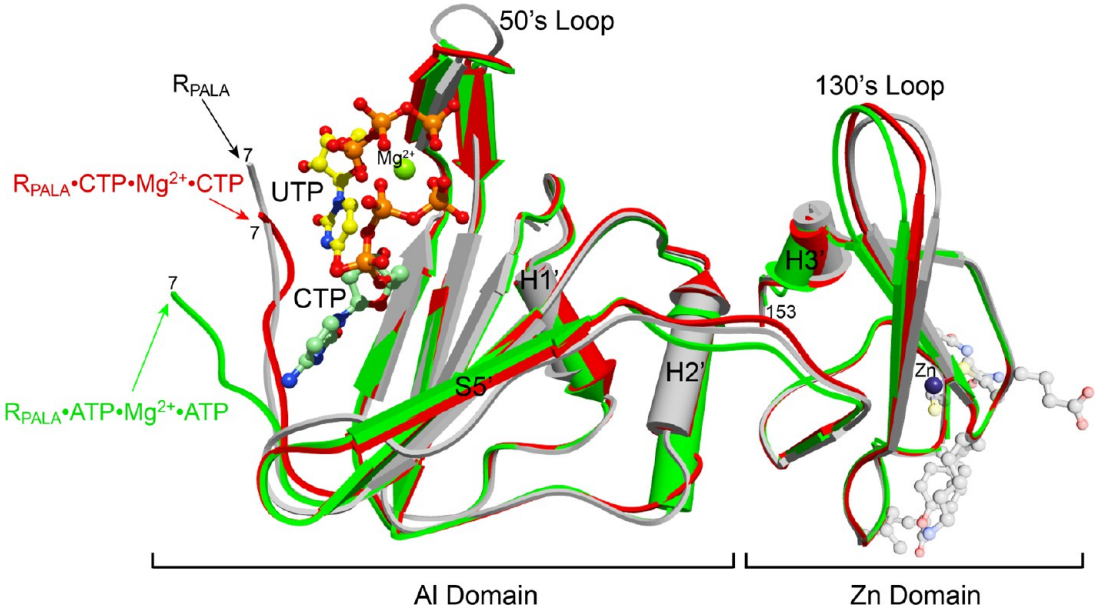

Figure 6. Structural changes induced by the binding of ATP + Mg^{2+} (green, R_{PALA}·ATP·Mg^{2+}·ATP) or CTP + UTP + Mg^{2+} (red, R_{PALA}·CTP·Mg^{2+}·UTP) to the unliganded r6 regulatory chain of ATCase in the R state (gray, R_{PALA}, PDB ID 1D09). The two structures with ligands were aligned to the structure in the absence of regulatory nucleotides. For clarity, the two ATPs and Mg^{2+} that are bound in the R_{PALA}·ATP·Mg^{2+}·ATP are not shown; however, they occupy positions very similar to CTP and UTP. The side chains of the r6 chain that interact via hydrogen bonding with the adjacent catalytic chain (c6) are shown with transparency on the right. The location of the N-terminal residue 7 and the C-terminal residue 153 are indicated.

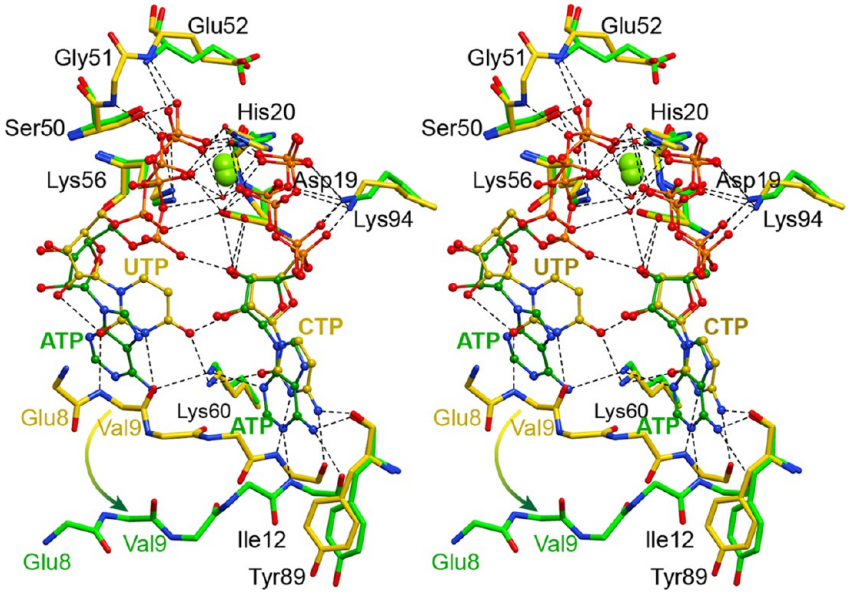

Figure 7. Stereoview comparison of the r6 regulatory site of ATCase from the R_{PALA}·ATP·Mg^{2+}·ATP (green carbons) and the R_{PALA}·CTP·Mg^{2+}·UTP (yellow carbons) structures. Hydrogen bonding interactions are shown with dotted lines. The arrow indicates the motion of the segment of the N-terminus shown.

UTP·Mg^{2+} to inhibit the enzyme. This displacement prevents an interaction between the uridine N3 and the backbone of Ile12. The uridine of the UTP in the B subsite is held by two interactions, each to the ε-amino group of Lys60 (see Figure 5F). The majority of the binding affinity comes from interactions of the triphosphate with the Mg^{2+} and the side chains of His20, Ser50, Lys56, and the backbone of Glu52. The side chain of Asp19 also has a water-mediated interaction that further adds to the triphosphate interactions (see Figure 5F).

Figure 6 compares the structural consequences of NTPs and Mg^{2+} binding to the allosteric site of the regulatory chain of ATCase. In this figure, the R_{PALA} structure without nucleotide effectors is compared with the R_{PALA}·ATP·Mg^{2+}·ATP and the R_{PALA}·CTP·Mg^{2+}·UTP structures. ATP·Mg^{2+} substantially activates the enzyme, while CTP·Mg^{2+}·UTP causes the most inhibition. The position of the N-terminal region of the regulatory chain is altered in the R_{PALA}·ATP·Mg^{2+}·ATP structure, as compared to the other two. As seen in Figure 7, the molecular basis for the alternation in position of the N-

dx.doi.org/10.1021/bi401205n | *Biochemistry* 2013, 52, 8036−8047

terminal region is due to the larger size of the purine ring of ATP as compared to the pyrimidine ring of UTP in the B subsite. In the R_{PALA}·CTP·Mg^{2+}·UTP structure, the carbonyl oxygen at the 2 position and the nitrogen at the 3 position of the pyrimidine ring interact with the backbone of Val9. However, in the R_{PALA}·ATP·Mg^{2+}·ATP structure, the purine ring of the ATP in the B subsite fits into the site by displacing the N-terminus.

Both structures with NTPs and Mg^{2+} have a significant shift in the 50s loop region, as residues from this loop (Ser50, Glu52, Lys56) interact with the NTP in the B subsite (see Figure 6). Strand S5′, part of the five-stranded sheet in the Al domain that bridges to the Zn domain, is shifted in both structures with NTPs and Mg^{2+}, as compared to the R_{PALA} structure. In the interface between the Al−Zn domains (strand S5′ and helix H2′), the shifts in the R_{PALA}·ATP·Mg^{2+}·ATP and the R_{PALA}·CTP·Mg^{2+}·UTP structures are in opposite directions. This alteration in the Al−Zn interface alters hydrophobic contacts that have been shown previously to be important for the allosteric regulation.[39,40] Notable is the lack of significant structural motions in the region around the structural Zn ion in the Zn domain, the region of the Zn domain that interacts with the adjacent catalytic chain. The C-terminal helix (Helix H3′) undergoes a dramatic reorientation resulting in alterations to the position of the C-terminus of the regulatory chain. The interactions between the C-terminus of the r1 chain and the c4 catalytic chain in the T state have been shown to be involved in allosteric regulation. For example, Xi et al.[41] have previously shown that the removal of two residues from the C-terminus of the regulatory chain is sufficient to abolish the ability of CTP to inhibit the enzyme.

Comparison of the Solution and Crystal structures of ATCase·PALA Complex in the Presence of ATP and Mg^{2+}·ATP. Structural information on the R state of ATCase in the presence of ATP and ATP·Mg^{2+} has been obtained using small-angle X-ray scattering in solution (SAXS). Fetler and Vachette[5] showed that the solution structure of ATCase·PALA (R_{SOL}) was altered in the presence of ATP and in the presence of ATP·Mg^{2+} to a larger extent. The SAXS data was then used to model the structures of the ATCase·PALA complex in the presence of ATP (R_{SOL}·ATP) and ATP·Mg^{2+} (R_{SOL}·ATP·Mg^{2+}). The R_{SOL}·ATP and the R_{SOL}·ATP·Mg^{2+} modeled structures were elongated along the 3-fold axis 2.8 and 4.4 Å more than the R_{PALA} crystal structure. Furthermore, the catalytic subunits of the R_{SOL}·ATP and the R_{SOL}·ATP·Mg^{2+} structures rotated 8° and 13° more around the 3-fold axis, and the regulatory subunits rotated 9° and 15° more around their respective 2-fold axes, respectively, than the R_{PALA} structure.

The structural changes proposed by Fetler and Vachette[5] are not observed when comparing the R_{PALA} crystal structure obtained in the absence of nucleotides[28] with the R_{PALA}·ATP and the R_{PALA}·ATP·Mg^{2+}·ATP crystal structures reported here. For both the R_{PALA}·ATP and R_{PALA}·ATP·Mg^{2+}·ATP structures, neither the expansion along the 3-fold axis nor the rotations of the subunits around the 3-fold and 2-fold axes differ significantly from that observed for the R_{PALA} structure without allosteric effectors. The structural models determined from the SAXS data[5] are inconsistent with the crystal structures, suggesting that the structure of the enzyme in solution is different from that in the crystal.

In order to investigate the discrepancy between the solution and crystal structures, we calculated SAXS profiles on the basis of the atomic positions determined by X-ray crystallography. As seen in Figure 8, the calculated SAXS profile for R_{PALA} without regulatory effectors is different from that calculated for the

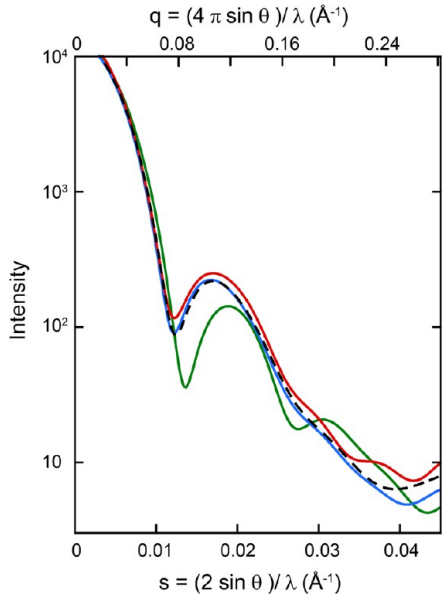

Figure 8. Calculated SAXS scattering curves of ATCase. SAXS profiles of the biological unit of ATCase were calculated using the FOXS Server[32] in the T state (green, PDB ID 1ZA1 with CTP removed) and R state with PALA (blue, PDB ID 1D09). Also shown are the calculated SAXS profiles for the R_{PALA}·ATP·Mg^{2+}·ATP structure with ligands (red) and the same structure with the ATP and Mg^{2+} atoms removed (black dashed).

R_{PALA}·ATP·Mg^{2+}·ATP structure. The largest difference in the SAXS patterns is in the region of the first subsidiary minimum and maximum, exactly as was observed experimentally.[5] However, if all the atoms constituting ATP and Mg^{2+} are removed from the R_{PALA}·ATP·Mg^{2+}·ATP coordinates and the SAXS pattern is recalculated, the pattern obtained is essentially identical to the pattern calculated for the R_{PALA} structure in the absence of allosteric effectors. These calculations indicate that the R_{SOL}·ATP and R_{SOL}·ATP·Mg^{2+} structures of ATCase reported by Fetler and Vachette[5] are incorrect, and that the observed difference in scattering between the R-state enzyme in the absence and presence of ATP and ATP·Mg^{2+} is due exclusively to the extra scattering caused by the bound ligands. These results also indicate that the solution and crystal structures of ATCase are virtually identical.

Nucleotide Site Specificity. The ATCase structures reported here confirm that the allosteric site on each regulatory chain of ATCase is actually a dinucleotide site composed of two subsites that can bind nucleotide triphosphates. Furthermore, the nucleotide that occupies each of the two independent sites must be considered in any model of allosteric regulation of ATCase. The A subsite can bind CTP, ATP, and UTP, while the B subsite can bind ATP and UTP. Although GTP has been shown to bind to the allosteric site,[15] its site specificity, or lack thereof, has not been established. The simultaneous binding of two nucleotides to the A and B subsites, in any combination, is dependent upon the presence of a divalent cation. In the absence of divalent cations, ATP and CTP bind with high affinity only to the A subsite (see Figure 5A,B). The only NTP that is able to bind to the B subsite with reasonable affinity in the absence of divalent cations is UTP.[6]

dx.doi.org/10.1021/bi401205n | Biochemistry 2013, 52, 8036−8047

The preferential binding of CTP to the A subsite and UTP to the B subsite is due to the interactions involving the functional group difference at the 4 position of the pyrimidine ring. The 4-keto group of uracil cannot interact with the A subsite because there are no appropriately positioned hydrogen-bond donors (see Figure 5F). However, the backbone carbonyls of Ile12 and Tyr89 serve as hydrogen-bond acceptors for the 4-amino group of the cytosine ring of CTP (see Figure 5E). The 6-amino group of adenine interacts with the same two groups on the enzyme to provide the specificity with respect to ATP (see Figure 5D).

In the presence of Mg^{2+}, ATP can occupy both the A and B subsites. When the two subsites are populated in this fashion the enzyme is more activated than when ATP is bound just to the A subsite (see Figure 2). The combination of CTP binding at the A subsite and UTP binding to the B subsite results in the highest level of inhibition of the enzyme. In fact, in the presence of Mg^{2+}, neither CTP nor UTP alone inhibit the enzyme significantly (see Figure 2). Cockrell and Kantrowitz[7] have described the selective binding of the nucleotides CTP and UTP to the A and B subsites, respectively. Part of the subsite selectivity is due to electrostatic interactions between the pyrimidine ring and Lys60, a residue that lies at the interface between the A and B subsites and has interactions with the nucleotides bound in each subsite. Therefore, an unfavorable electrostatic interaction between Lys60 and the 4-amino group of CTP precludes the binding of CTP to the B subsite. It is likely that the CTP·Mg^{2+} complex has a lower binding affinity to the allosteric site than CTP, and this fact explains why 2 mM CTP·Mg^{2+} does not inhibit the enzyme. The structural basis for the ability of ATP to bind to both the A and B subsites can also be ascribed to electrostatic interactions between ATP and Lys60. The adenine N3 of ATP in the A subsite interacts with Lys60, and in the B subsite Lys60 interacts with N7 and the 6-amino group, all of which bear a partial negative charge.[42]

Role of the N-termini of the Regulatory Chains of ATCase in Allosteric Regulation. In most structures of wild-type and mutant versions of ATCase, the N-termini of the regulatory chains are disordered to a significant extent to make the determination of the atomic positions of the residues impossible. Depending upon the structure, between 1 and 10 residues have been excluded. Part of the reason for the disordered N-termini is that this part of the protein makes interactions with the nucleotide in the B subsite, structures of which have not been available. The R_{PALA}·CTP·Mg^{2+}·UTP and R_{PALA}·ATP·Mg^{2+}·ATP structures reported here correspond to highly inhibited and activated forms of the enzyme, respectively. As discussed above, in these two structures, the N-terminal region of the regulatory chains exhibit completely different conformations.

Shown in Figure 9A are the allosteric domains of the regulatory subunit of the R_{PALA}·CTP·Mg^{2+}·UTP structure. The N-termini of the r1 and r6 chains are parallel to one another at the dimer interface. Shown in Figure 9B are the allosteric domains of the regulatory subunit of the R_{PALA}·ATP·Mg^{2+}·ATP structure. The larger purine ring of ATP in the A subsite displaces the N-terminus of the r1 chain into the allosteric site of the r6 chain and interacts with the ATP bound in the B subsite of the r6 chain and vice versa. The penetration of the N-terminal region into the opposing regulatory chain positions Lys6 to help neutralize the negative charges on the two triphosphates. Additional stabilization of the nucleotide in the B subsite is provided by hydrophobic interactions with Leu7 and Val9. The crossover of the N-terminal region into the opposite regulatory chain of the dimer is particularly intriguing, as this would enhance the strength of the interface between the regulatory chains within the regulatory dimer, providing a new mode by which ATP can stabilize the R state of ATCase. The position of the N-termini in the R_{PALA}·CTP·Mg^{2+}·UTP structure would provide no added stabilization to this interface, thus neutralizing the effect of ATP and by inference, destabilizing the R state.

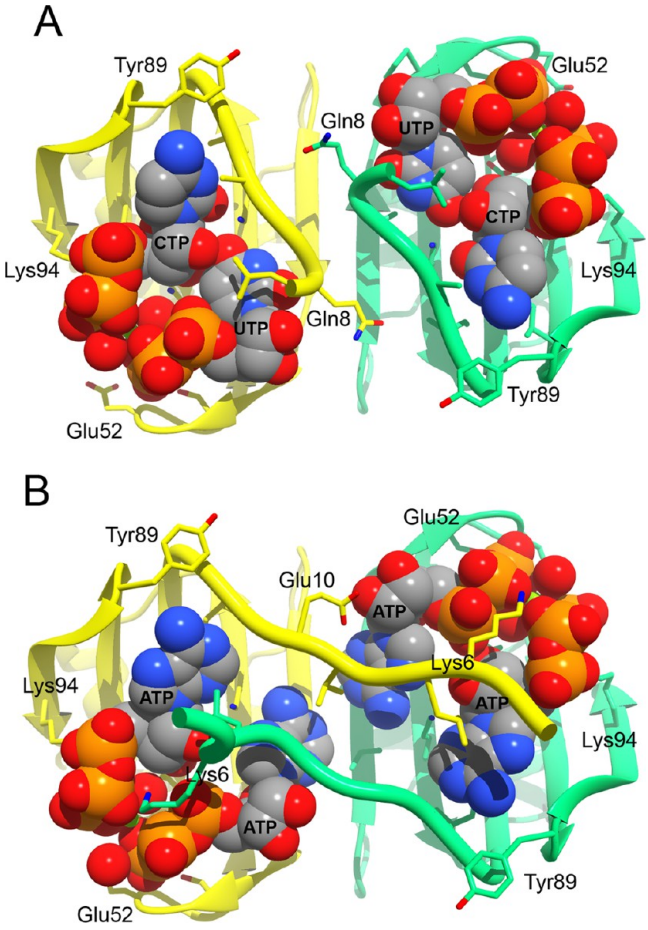

Figure 9. Alternate conformations of the N-terminal region. The R_{PALA}· CTP·Mg^{2+}·UTP (A) and R_{PALA}·ATP·Mg^{2+}·ATP (B) structures showing the allosteric domains of the regulatory subunit. In (A), the N-termini curl around and interact with the B subsite within their own chain, while in (B), the N-termini of one regulatory chain penetrates into the B subsite of the other regulatory chain. In the R_{PALA}·CTP·Mg^{2+}·UTP and R_{PALA}·ATP·Mg^{2+}·ATP structures, six and three residues were omitted from the N-termini due to weak electron density. Figure S2 shows the relationship of the portion of the regulatory subunit shown in this figure to the holoenzyme.

Allosteric Regulation is Governed by Both Subsites in Each Regulatory Chain of ATCase. Previous kinetic studies of single amino acid substitutions have been performed on residues identified here as involved in nucleotide binding to the A and B subsites. In the A subsite, Lys94[43] is critical for nucleotide binding. Residues that interact with the nucleotide in both subsites include Asp19, His20, and Lys60. The K60A mutation eliminates CTP inhibition and reduces the affinity of ATP. The mutant enzymes D19A,[44] H20A,[45] and K56A[46] lose their ability to be inhibited synergistically by UTP in the presence of CTP. The loss of synergistic inhibition could not

dx.doi.org/10.1021/bi401205n | Biochemistry 2013, 52, 8036−8047

previously be explained from a structural perspective, especially for the K56A mutation as the B subsite had not been discovered. As seen in Figure 5D, Asp19, His20, and Lys56 all provide stabilizing interactions to the ATP bound in the B subsite and have few or no interactions with CTP bound in the A subsite. Mutations at residues Asp4, Lys6, and Leu7 of the N-terminal region of the regulatory chain all influence the regulatory properties of the enzyme.[47] As seen in Figure 9, Leu7 is involved in a hydrophobic interaction with either the purine or pyrimidine ring of bound nucleotides, and Lys6 helps to neutralize the charge of the two triphosphates in the R_{PALA}·ATP·Mg^{2+}·ATP structure (Figure 5D). These site-specific amino acid substitutions provide functional evidence that both the A and B subsites play a role in the allosteric regulation of ATCase.

New Model of Allosteric Regulation of ATCase Involving a Dinucleotide Binding Site. Based upon the kinetics and the five X-ray structures reported here, along with the previously reported R_{PALA}·UTP,[6] T·dCTP·Mg^{2+}·UTP and T·CTP·Mg^{2+}·UTP structures,[7] a new model of allosteric regulation of ATCase can be proposed: (1) Each regulatory chain of ATCase can bind two nucleotides simultaneously but only in the presence of a divalent cation such as Mg^{2+} (see Figure 5D–F). (2) Reports from the last 57 years stating that CTP is the allosteric feedback inhibitor of ATCase are inaccurate. Although CTP in the absence of divalent cations can inhibit the enzyme, in the presence of M^{2+} ions at or below physiological concentrations, CTP does not significantly inhibit the enzyme. Reports from the last 24 years that ATCase is synergistically inhibited by UTP in the presence of CTP are incorrect. In the absence of metals, the combination of CTP and UTP does not inhibit the enzyme more than CTP alone (see Figure 2). In the presence of a Mg^{2+}, Ca^{2+}, or Zn^{2+} at concentrations less than intracellular (2 mM), CTP does not significantly inhibit ATCase (see Figure 2 and Table 1). In the presence of Mg^{2+}, Ca^{2+}, or Zn^{2+} at concentrations below physiological, the allosteric inhibitor of ATCase is the combination of CTP·M^{2+}·UTP with CTP binding to the A subsite and UTP binding to the B subsite. Thus, both end products of the pyrimidine pathway, CTP and UTP, act together to feedback inhibit ATCase. (3) Although ATCase can be activated by the binding of ATP in the absence of divalent cations, the enzyme can be activated to a larger extent by ATP·M^{2+}. Although GTP was never thought to play a significant role in allosteric regulation of ATCase, it can function in conjunction with ATP·Mg^{2+} (see Figures 2 and 3). Thus, both end products of the purine pathway, ATP and GTP, can act together to allosterically activate ATCase. (4) The conformation of the N-termini of the regulatory chains is governed by the nucleotides bound in the A and B subsites. The inhibited form of the enzyme with CTP·Mg^{2+}·UTP bound exhibits an intrachain orientation of the N-termini, while the activated form of the enzyme with ATP·Mg^{2+}·ATP bound exhibits an interchain orientation of the N-termini. Thus, the activated form of the enzyme has increased stabilization of the interface between the two chains of the regulatory dimer, suggesting that these interfaces are functionally important for the stabilization of the T and R states of ATCase. This selective stabilization of the T and R states provides an explanation for how the nucleotides function in the activation and inhibition of ATCase that is consistent with the model of allostery proposed by Monod, Wyman, and Changeux.[48]

■ ASSOCIATED CONTENT

Supporting Information

Tables S1 and S2 and Figures S1 and S2. This material is available free of charge via the Internet at http://pubs.acs.org.

■ AUTHOR INFORMATION

Corresponding Author

*E-mail: evan.kantrowitz@bc.edu. Tel.: (617) 552-4558.

Funding

This work was supported in part by Grant GM26237 from the National Institutes of Heath. Data for three of the structures were measured at Beamline X29 of the National Synchrotron Light Source. Use of the National Synchrotron Light Source, Brookhaven National Laboratory, was supported by the U.S. Department of Energy, Office of Science, Office of Basic Energy Sciences, under Contract No. DE-AC02–98CH10886.

Notes

The authors declare no competing financial interest.

■ ACKNOWLEDGMENTS

We thank H. Robinson of Brookhaven National Laboratory for data collection and assistance with data processing and K. M. Harris for critically proofreading the manuscript.

■ ABBREVIATIONS

ATCase, aspartate transcarbamoylase; CP, carbamoyl phosphate; RMSD, root-mean-square deviation; PALA, *N*-phosphonoacetyl-L-aspartate; 50s loop, residues 46–58 of the regulatory chain; 130s loop, residues 129–134 of the regulatory chain; c1 and c6, catalytic chains in the asymmetric unit; r1 and r6, regulatory chains of a dimer in the asymmetric unit; PDB, Protein Data Bank

■ REFERENCES

(1) Reichard, P., and Hanshoff, G. (1956) Aspartate Carbamyl Transferase from *Escherichia coli*. *Acta Chem. Scand. 10*, 548–560.

(2) Fetler, L., Kantrowitz, E. R., and Vachette, P. (2007) Direct Observation in Solution of Pre-Existing Structure Equilibrium for a Mutant of Allosteric Aspartate Transcarbamoylase. *Proc. Natl. Acad. Sci. U.S.A. 104*, 495–500.

(3) Macol, C. P., Tsuruta, H., Stec, B., and Kantrowitz, E. R. (2001) Direct Structural Evidence for a Concerted Allosteric Transition in *Escherichia coli* Aspartate Transcarbamoylase. *Nat. Struct. Biol. 8*, 423–426.

(4) Wild, J. R., Loughrey-Chen, S. J., and Corder, T. S. (1989) In the Presence of CTP, UTP Becomes an Allosteric Inhibitor of Aspartate Transcarbamylase. *Proc. Natl. Acad. Sci. U.S.A. 86*, 46–50.

(5) Fetler, L., and Vachette, P. (2001) The Allosteric Activator Mg-ATP Modifies the Quaternary Structure of the R-State of *Escherichia coli* Aspartate Transcarbamylase without Altering the TR Equilibrium. *J. Mol. Biol. 309*, 817–832.

(6) Peterson, A. W., Cockrell, G. M., and Kantrowitz, E. R. (2012) A Second Allosteric Site in *E. coli* Aspartate Transcarbamoylase. *Biochemistry 51*, 4776–4778.

(7) Cockrell, G. M., and Kantrowitz, E. R. (2012) Metal Ion Involvement in the Allosteric Mechanism of *Escherichia coli* Aspartate Transcarbamoylase. *Biochemistry 51*, 7128–7137.

(8) Howlett, G. J., Blackburn, M. N., Compton, J. G., and Schachman, H. K. (1977) Allosteric Regulation of Aspartate Transcarbamoylase. Analysis of the Structural and Functional Behavior in Terms of a Two-State Model. *Biochemistry 16*, 5091–5099.

(9) London, R. E., and Schmidt, P. G. (1972) A Model for Nucleoside Regulation of Aspartate Transcarbamylase. *Biochemistry 11*, 3136–3142.

(10) Suter, P., and Rosenbusch, J. P. (1977) Asymmetry of Binding and Physical Assignments of CTP and ATP Sites in Aspartate Transcarbamoylase. *J. Biol. Chem. 252*, 8136−8141.
(11) Changeux, J., Gerhart, J., and Schachman, H. (1968) Allosteric Interactions in Aspartate Transcarbamylase. I. Binding of Specific Ligands to the Native Enzyme and Its Isolated Subunits. *Biochemistry 7*, 531−538.
(12) Kim, K. H., Pan, Z., Honzatko, R. B., Ke, H.-M., and Lipscomb, W. N. (1987) Structural Asymmetry in the CTP-Liganded Form of Aspartate Carbamoyltransferase from *Escherichia coli*. *J. Mol. Biol. 196*, 853−875.
(13) Winlund, C. C., and Chamberlin, M. J. (1970) Binding of Cytidine Triphosphate to Aspartate Transcarbamylase. *Biochem. Biophys. Res. Commun. 40*, 43−49.
(14) Matsumoto, S., and Hammes, G. G. (1973) Equilibrium Binding Study of the Interaction of Aspartate Transcarbamoylase with Cytidine 5′-Triphosphate and Adenosine 5′-Triphosphate. *Biochemistry 12*, 1388−1394.
(15) Mendes, K. R., Martinez, J. A., and Kantrowitz, E. R. (2010) Asymmetric Allosteric Signaling in Aspartate Transcarbamoylase. *ACS Chem. Biol. 5*, 499−506.
(16) Gray, C. W., Chamberlin, M., and Gray, D. (1973) Interaction of Aspartate Transcarbamylase with Regulatory Nucleotides. *J. Biol. Chem. 248*, 6071−6079.
(17) Suter, P., and Rosenbusch, J. P. (1976) Determination of Ligand Binding: Partial and Full Saturation of Aspartate Transcarbamylase. Applicability of a Filter Assay to Weakly Binding Ligands. *J. Biol. Chem. 251*, 5986−5991.
(18) Suter, P., and Rosenbusch, J. P. (1976) Heterogeneity of Sites in Isolated Catalytic Subunits of Aspartate Transcarbamoylase. *Eur. J. Biochem. 70*, 191−196.
(19) Gerhart, J. C., and Pardee, A. B. (1962) Enzymology of Control by Feedback Inhibition. *J. Biol. Chem. 237*, 891−896.
(20) Nowlan, S. F., and Kantrowitz, E. R. (1985) Superproduction and Rapid Purification of *E. coli* Aspartate Transcarbamoylase and Its Catalytic Subunit under Extreme Derepression of the Pyrimidine Pathway. *J. Biol. Chem. 260*, 14712−14716.
(21) Baker, D. P., and Kantrowitz, E. R. (1993) The Conserved Residues Glutamate-37, Aspartate-100 and Arginine-269 Are Important for the Structural Stabilization of *Escherichia coli* Aspartate Transcarbamoylase. *Biochemistry 32*, 10150−10158.
(22) Gerhart, J. C., and Holoubek, H. (1967) The Purification of Aspartate Transcarbamylase of *Escherichia coli* and Separation of Its Protein Subunits. *J. Biol. Chem. 242*, 2886−2892.
(23) Bock, R. M., Ling, N. S., Morell, S. A., and Lipton, S. H. (1956) Ultraviolet Absorption Spectra of Adenosine-5′-Triphosphate and Related 5′-Ribonucleotides. *Arch. Biochem. Biophys. 62*, 253−264.
(24) Pastra-Landis, S. C., Foote, J., and Kantrowitz, E. R. (1981) An Improved Colorimetric Assay for Aspartate and Ornithine Transcarbamylases. *Anal. Biochem. 118*, 358−363.
(25) Krause, K. L., Voltz, K. W., and Lipscomb, W. N. (1987) 2.5 Å Structure of Aspartate Carbamoyltransferase Complexed with the Bisubstrate Analog *N*-(phosphonacetyl)-L-aspartate. *J. Mol. Biol. 193*, 527−553.
(26) Otwinowski, Z., and Minor, W. (1997) in *Methods Enzymol.* (Carter, C. W., Jr., Sweet, R. M., Eds.), pp 307−326, Academic Press, New York.
(27) Pflugrath, J. W. (1999) The Finer Things in X-Ray Diffraction Data Collection. *Acta Crystallogr. D55*, 1718−1725.
(28) Jin, L., Stec, B., Lipscomb, W. N., and Kantrowitz, E. R. (1999) Insights into the Mechanism of Catalysis and Heterotropic Regulation of *E. coli* Aspartate Transcarbamoylase Based upon a Structure of Enzyme Complexed with the Bisubstrate Analog *N*-phosphonacetyl-L-aspartate at 2.1 Å. *Proteins: Struct., Funct., Genet. 37*, 729−742.
(29) Adams, P. D., Afonine, P. V., Bunkóczi, G., Chen, V. B., Davis, I. W., Echols, N., Headd, J. J., Hung, L.-W., Kapral, G. J., Grosse-Kunstleve, R. W., McCoy, A. J., Moriarty, N. W., Oeffner, R., Read, R. J., Richardson, D. C., Richardson, J. S., Terwilliger, T. C., and Zwart, P. H. (2010) PHENIX: A Comprehensive Python-Based System for Macromolecular Structure Solution. *Acta Crystallogr. D66*, 213−221.
(30) Emsley, P., Lohkamp, B., Scott, W. G., and Cowtan, K. (2010) Features and Development of Coot. *Acta Crystallogr. D66*, 486−501.
(31) Laskowski, R. A., MacArthur, M. W., Moss, D. S., and Thornton, J. M. (1993) PROCHECK: A Program to Check the Stereochemical Quality of Protein Structures. *J. Appl. Crystallogr. 26*, 283−291.
(32) Schneidman-Duhovny, D., Hammel, M., and Sali, A. (2010) FoXS: A Web Server for Rapid Computation and Fitting of Saxs Profiles. *Nucleic Acids Res. 38* (Suppl), W540−544.
(33) Christopherson, R. I., and Finch, L. R. (1977) Regulation of Aspartate Carbamoyltransferase of *Escherichia coli* by the Interrelationship of Magnesium and Nucleotides. *Biochim. Biophys. Acta 481*, 80−85.
(34) Honzatko, R. B., Lauritzen, A. M., and Lipscomb, W. N. (1981) Metal Cation Influence on Activity and Regulation of Aspartate Carbamoyltransferase. *Proc. Natl. Acad. Sci. U.S.A. 78*, 898−902.
(35) Buckstein, M. H., He, J., and Rubin, H. (2008) Characterization of Nucleotide Pools as a Function of Physiological State in Escherichia Coli. *J. Bacteriol. 190*, 718−726.
(36) Kung, F. C., Raymond, J., and Glaser, D. A. (1976) Metal Ion Content of *Escherichia coli* versus Cell Age. *J. Bacteriol. 126*, 1089−1095.
(37) Stieglitz, K., Stec, B., Baker, D. P., and Kantrowitz, E. R. (2004) Monitoring the Transition from the T to the R State in *E. coli* Aspartate Transcarbamoylase by X-Ray Crystallography: Crystal Structures of the E50A Mutant in Four Distinct Allosteric States. *J. Mol. Biol. 341*, 853−868.
(38) Gerhart, J. C. (1970) A Discussion of the Regulatory Properties of Aspartate Transcarbamylase From *Escherichia coli*. *Curr. Top. Cell. Regul. 2*, 275−325.
(39) Van Vliet, F., Xi, X.-G., DeStaercke, C., DeWannemaeker, B., Jacobs, A., Cherfils, J., Ladjimi, M. M., Hervé, G., and Cunin, R. (1991) Heterotropic Interactions in Aspartate Transcarbamoylase: Turning Allosteric ATP Activation into Inhibition as a Consequence of a Single Tyrosine to Phenylalanine Mutation. *Proc. Natl. Acad. Sci. U.S.A. 88*, 9180−9183.
(40) Xi, X.-G., DeStaercke, C., Van Vliet, F., Triniolles, F., Jacobs, A., Stas, P. P., Ladjimi, M. M., Simon, V., Cunin, R., and Hervé, G. (1994) The Activation of *Escherichia coli* Aspartate Transcarbamylase by ATP: Specific Involvement of Helix H2′ at the Hydrophobic Interface between the Two Domains of the Regulatory Chains. *J. Mol. Biol. 242*, 139−149.
(41) Xi, X.-G., Van Vliet, F., Ladjimi, M. M., DeWannemaeker, B., DeStaercke, C., Glansdorff, N., Piérard, A., Cunin, R., and Hervé, G. (1991) The Heterotropic Interactions in Aspartate Transcarbamoylase: Subunit Interfaces Involved in CTP Inhibition and ATP Activation. *J. Mol. Biol. 220*, 789−799.
(42) Abraham, R. J., and Smith, P. E. (1988) Charge Calculations in Molecular Mechanics 6: The Calculation of Partial Atomic Charges in Nucleic Acid Bases and the Electrostatic Contribution to DNA Base Pairing. *Nucleic Acids Res. 16*, 2639−2657.
(43) Zhang, Y., Ladjimi, M. M., and Kantrowitz, E. R. (1988) Site-Directed Mutagenesis of a Residue Located in the Regulatory Site of *Escherichia coli* Aspartate Transcarbamylase. *J. Biol. Chem. 263*, 1320−1324.
(44) Zhang, Y., and Kantrowitz, E. R. (1991) The Synergistic Inhibition of *Escherichia coli* Aspartate Carbamoyltransferase by UTP in the Presence of CTP Is Due to the Binding of UTP to the Low Affinity CTP Sites. *J. Biol. Chem. 266*, 22154−22158.
(45) Zhang, Y., and Kantrowitz, E. R. (1992) Probing the Regulatory Site of *Escherichia coli* Aspartate Transcarbamoylase by Site-Specific Mutagenesis. *Biochemistry 31*, 792−798.
(46) Corder, T. S., and Wild, J. R. (1989) Discrimination between Nucleotide Effector Responses of Aspartate Transcarbamoylase Due to a Single Site Substitution in the Allosteric Binding Site. *J. Biol. Chem. 264*, 7425−7430.
(47) Dembowski, N. J., and Kantrowitz, E. R. (1994) The Use of Alanine Scanning Mutagenesis To Determine the Role of the Amino

Terminus of the Regulatory Chain in the Heterotropic Mechanism of *Escherichia coli* Aspartate Transcarbamoylase. *Protein Eng. 7*, 673−679.
(48) Monod, J., Wyman, J., and Changeux, J. P. (1965) On the Nature of Allosteric Transitions: A Plausible Model. *J. Mol. Biol. 12*, 88−118.
(49) Pettersen, E. F., Goddard, T. D., Huang, C. C., Couch, G. S., Greenblatt, D. M., Meng, E. C., and Ferrin, T. E. (2004) UCSF Chimera—A Visualization System for Exploratory Research and Analysis. *J. Comput. Chem. 25*, 1605−1612.